Koyama, D., Dale, H. J. A., & Orr-Ewing, A. J. (2018). Ultrafast Observation of a Photoredox Reaction Mechanism: Photoinitiation in Organocatalyzed Atom-Transfer Radical Polymerization. *Journal of the American Chemical Society*, *140*(4), 1285-1293. https://doi.org/10.1021/jacs.7b07829

Ultrafast Observation of a Photoredox Reaction Mechanism: Photo-initiation in Organocatalyzed Atom-Transfer Radical Polymerization

Daisuke Koyama[1], Harvey J. A. Dale[1] and Andrew J. Orr-Ewing*

School of Chemistry, University of Bristol, Cantock's Close, Bristol, BS8 1TS, UK

* Author for correspondence: a.orr-ewing@bristol.ac.uk

Abstract

Photoredox catalysis has driven a revolution in the field of organic chemistry, but direct mechanistic insights into reactions of genuine synthetic utility remain relatively scarce. Herein we report ultrafast time-resolved spectroscopic observation of a bimolecular organocatalysed photoredox reaction, from catalyst photoexcitation through to photoinduced electron transfer (PET) and intermediate formation, using transient vibrational and electronic absorption spectroscopy with sub-picosecond time resolution. Specifically, the photochemical dynamics of initiation in organocatalysed atom-transfer radical polymerization (O-ATRP) are elucidated for two complementary photoredox organocatalysts (N,N-diaryl-5,10-dihydrophenazines). Following photoexcitation, a dissociative bimolecular electron transfer is observed from the first excited singlet state of both photocatalysts to methyl 2-bromopropionate in dichloromethane, toluene and dimethylformamide. The photocatalyst excited donor state, ground state and radical cation are tracked in real time alongside the debrominated radical fragment. Our work challenges previously proposed mechanisms of initiation in O-ATRP, and indicates that PET from short-lived excited singlet states can exert control of polymer molecular weight and dispersity by supressing the steady-state concentration of the reactive debrominated radical. More broadly, we aim to demonstrate the potential of ultrafast absorption spectroscopy to observe directly transient, open-shell intermediates in mechanistic studies of photoredox catalysis.

[1] DK and HJAD contributed equally to this work.

Introduction

Photoredox catalysis exploits the notion that closed-shell molecules become more potent electron donors and electron acceptors when promoted to an excited electronic state. The photoexcitation of such species can be used to promote electron transfers that would otherwise not be thermodynamically viable in the ground electronic state. Exceptional advances in photoredox catalysis have been made in the last decade under the umbrella of synthetic organic chemistry, with the recent resurgence in this area often ascribed to pioneering research by the groups of MacMillan, Yoon, and Stephenson.[1-3] This work, and much that followed, has turned to the tris(bipyridine) complexes of $[Ru(bpy)_3]^{2+}$ and $[Ir(bpy)_3]^{3+}$ and their analogues as the photocatalysts (PCs) of choice. The photophysics of these transition metal complexes is well characterized,[4-5] and they have since been applied as PCs to a range of problems across synthetic organic chemistry, including the total synthesis of natural products,[6-8] heterocycle synthesis and functionalization,[9] asymmetric protocols[10] and the preparation of carbon-centered radicals.[11-13] They have also been used in the photocatalytic reduction of carbon dioxide to methane[14] and in the development of cooperative catalysis.[15-22] To circumvent the problems of natural scarcity and toxicity associated with the transition metals in these photoredox systems,[23-24] researchers are replacing metal-based catalysts with highly conjugated organocatalysts;[25-27] applications, and associated mechanistic studies, include oxidation using molecular oxygen,[28-30] cross-coupling,[31] cyanation,[32] addition to alkenes,[33] trifluoromethylation,[34] hydroxylation,[35] *N*-formylation,[36] and sulfinylation.[37]

In addition to these synthetic uses, selected organic PCs such as perylene, phenothiazine, dihydrophenazine and phenoxazine derivatives have recently been applied in the development of organocatalysed atom-transfer radical polymerization (O-ATRP).[38-41] Initiation in O-ATRP depends upon the reductive dehalogenation of an alkyl halide initiator *via* an outer-sphere electron transfer from a photoexcited organocatalyst; this process forms a reactive radical species, which instigates the propagation stage of polymerization. Low dispersity and control over the polymer molecular weight are thought to be promoted by keeping the concentration of this radical low.[42] Miyake and co-workers recently proposed an oxidative quenching pathway for O-ATRP with N,N'-diaryl-5,10-dihydrophenazines,[40-41] postulating that the first excited triplet state $^3PC^*(T_1)$ is responsible for the PET to the initiator (e.g. methyl 2-bromopropionate, MBP). The electron

transfer is dissociative, forming a dehalogenated radical fragment ($^2MP^{\cdot}$) and an ionic complex ($^2PC^{\cdot+}Br^-$), and termination of the polymerization supposedly occurs *via* a bimolecular, thermally mediated back electron transfer (**Scheme 1**).[43] They subsequently posited that the PCs most capable of efficiently mediating O-ATRP, and of affording the greatest control over polymer molecular weight and dispersity, are those whose excited states exhibit substantial intramolecular charge transfer (CT) character. The source of such control, they suggested, is that CT character in the excited donor state minimizes fluorescence and enhances electron transfer rates. They further investigated effects of solvents and irradiation energy on resulting polymer properties.[44-45] However, there is scope for more detailed study of these O-ATRP mechanisms to establish a firmer basis for interpretation of the existing observations.

In photoredox reactions using metal complexes, it is widely-accepted that long-lived T_1 states with metal-to-ligand CT character, populated with high quantum yield by efficient intersystem crossing (ISC), are responsible for PET.[24] The photochemical properties of the organic PCs (e.g., their redox potential, ISC quantum yields, and excited state lifetimes), as well as the polymerization conditions used in O-ATRP (e.g., the amount of photocatalyst required) significantly differ from those for the metal-centered photocatalysts, and their reaction mechanism may therefore also differ. For example, synthetic studies with phenyl phenothiazines have led researchers to contend that the first excited singlet state $^1PC^*(S_1)$, as opposed to $^3PC^*(T_1)$, may be responsible for the photoinduced electron transfer step.[46] In contrast, a recent spectroscopic study concluded that the majority of the PET (~89%) took place from T_1 state,[47] but was conducted at initiator concentrations 5 – 10 times lower than used for O-ATRP conditions.[40] Exhaustive mechanistic work by Matyjaszewski and co-workers with phenyl phenothiazine photocatalysts further emphasized the importance of the radical cation lifetime and the termination stage. These authors argued that stable radical cations with long lifetimes are required for controlled polymerization.[48] We show here that unravelling the mechanisms of organic photoredox catalysis can benefit from scrutiny by ultrafast transient absorption spectroscopy, which tracks the abundances of both the excited electronic states of the PC *and* reactive open-shell intermediates directly on timescales from sub-picosecond upwards, using the temporal evolution of their absorption signatures.

Several previous transient spectroscopy studies have examined photoinduced electron transfer (PET) reactions in solution.[49] However, this prior work has largely focussed either on

intramolecular PETs, in which the electron donor and acceptor are covalently tethered, or on intermolecular PETs that result in charge separation and recombination without the prospect of subsequent atom-transfer or onward reactivity. Ultrafast spectroscopy has previously been used to investigate the nature of the nascent ion-pair, quenching pathways, and the Marcus inversion region in bimolecular PETs.[50-51] Herein, we demonstrate an alternative application as a broader mechanistic tool to address the growing prominence of organic photoredox catalysis in synthesis. Vauthey and co-workers recently reported the use of ultrafast transient vibrational absorption spectroscopy (TVAS) to observe the photophysical relaxation of Ru(II) complexes,[52] but the current study explores both the intramolecular relaxation of an organic photocatalyst and its subsequent bimolecular reactions.

The photochemical dynamics of O-ATRP initiation by N,N'-diaryl-5,10-dihydrophenazine PCs were investigated using both TVAS and transient electronic absorption spectroscopy (TEAS) with sub-picosecond time resolution. Interpretation of the experimental data was supported by Kohn-Sham density functional theory (KS-DFT), time-dependent density functional theory (TD-DFT) and highly correlated *ab initio* SA-CASSCF/CASPT2 calculations. We consider two complementary photocatalysts based on the N,N'-diaryl-5,10-dihydrophenazine framework: N,N'-diphenyl-5,10-dihydrophenazine (PCH) and 5,10-di(4-trifluoromethylphenyl)-5,10-dihydrophenazine (PCF). These PCs were selected to test the mechanistic postulates of Miyake and co-workers, because the emissive state in PCH has local excitation (LE, π-π^*) character, whereas in PCF it has substantial intramolecular CT character, as deduced from solvatochromic effects in emission.[43] To balance spectroscopic convenience with synthetic applicability, we pursued experiments with three solvents: dichloromethane (DCM), toluene and dimethylformamide (DMF). The outcomes offer a complete picture of the early time dynamics of all the key intermediates in the PET process, and because some of our findings challenge previous mechanistic interpretations,[40-41] we accordingly propose some desirable properties of organic photocatalysts for O-ATRP.

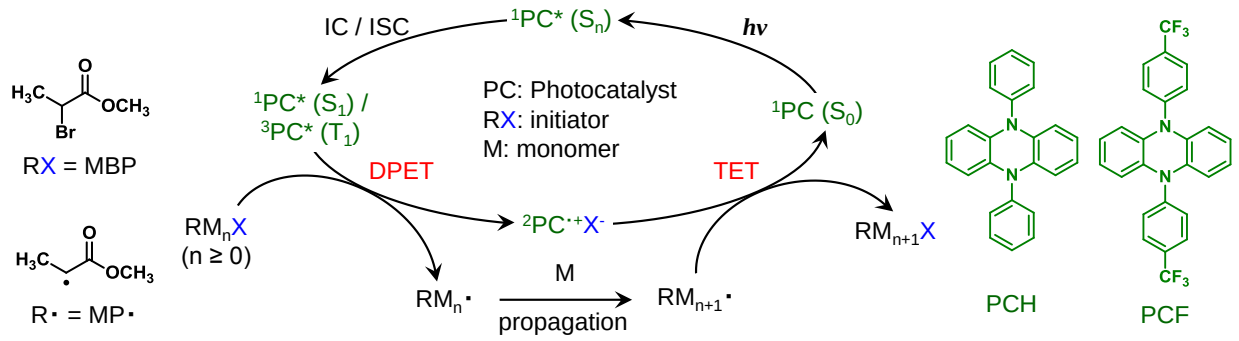

Scheme 1: Organic photoredox catalysis of atom-transfer radical polymerization. The photocatalytic cycle for O-ATRP with N,N'-diaryl-dihydrophenazines (PC) and alkyl bromide initiators, with electron transfer either from the S_1 or T_1 state of the photocatalyst. IC = Internal conversion. ISC = Intersystem crossing. DPET = Dissociative photoinduced electron transfer. TET = Thermal electron transfer. The chemical structures of the PCs used in this study are shown on the right.

Methods

All the TVAS and TEAS experiments reported here were conducted with an ultrafast laser system configured for pump-probe measurements. A Coherent Vitara-S Ti:Sapphire oscillator was used in conjunction with a Coherent Legend Elite HE+ regenerative amplifier to generate a single train of parent pulses with a repetition rate of 1 kHz. Each pulse was characterized by an average duration of τ = 40 fs, a carrier wavelength of λ_0 = 800 nm and an energy of ~5 mJ. The parent beam was split along three separate pathways; two beams of 2.45 mJ pulses were directed into Coherent OPerA Solo optical parametric amplifiers (OPAs) to generate UV pump and IR probe pulses (for TVAS), while a single train of 100 μJ pulses was diverted into a CaF_2 window to generate a broadband white light supercontinuum probe (for TEAS). In TEAS and TVAS, the UV pump wavelength was set to 370 nm and the pulses were characterized by an average energy of 600 nJ at the sample. Solutions were prepared to the desired concentration in a 10 mL amber glass volumetric flask and connected to a stainless steel Harrick flow cell *via* PTFE tubing. Two CaF_2 windows were sealed to the Harrick cell body by Kalrez O-rings and were separated by a pair of PTFE spacers of 380 μm (TVAS) or 500 μm (TEAS) thickness. The solution was flowed continuously through the cell using a peristaltic pump, to ensure that consecutive pump and probe

pulses sampled fresh regions of the solution. Further details are presented in the ESI, alongside computational and synthetic methodologies. Photocatalyst concentrations of 2.1 mmol dm^{-3} and initiator concentrations of 0.4 – 2.6 mol dm^{-3} were employed throughout the study. These compare with concentrations of 5 – 10 mmol dm^{-3} for the photocatalysts and 0.05 – 0.1 mol dm^{-3} for the initiator in O-ATRP studies by Miyake and co-workers.[40]

Results and Discussion

Steady-State Characterization

The organocatalysts N,N'-diphenyl-5,10-dihydrophenazine and 5,10-di(4-trifluoromethylphenyl)-5,10-dihydrophenazine exhibit intriguing photophysical behavior. In both molecules, the lowest-energy optically bright transition occurs with a maximum absorbance at 370 nm. TD-DFT calculations indicate that at this wavelength both PCH (D_{2h}) [$S_0(A_g) \rightarrow S_2(B_{2u})$] and PCF ($C_{2h}$) [$S_0(A_g) \rightarrow S_4(B_u)$] undergo photoexcitation to a state with primarily LE character (π-π^*) in the Franck-Condon region (Figure S7 and S9 of Supporting Information (SI)). The maximum in the emission band of PCH is recorded at a wavelength of 480 nm, independent of solvent,[41] whereas emission from PCF exhibits substantial solvatochromic shifts, with wavelengths of maximum emission varying from 480 – 650 nm depending upon solvent polarity (Figure S4), in agreement with a prior report.[43] The steady-state emission intensity from PCF is essentially unchanged upon the addition of triplet quenchers 2,5-dimethylhexa-2,4-diene (E_{T1} = 176 kJ mol^{-1} [53]), cyclohexa-1-3-diene (E_{T1} = 219 kJ mol^{-1} [54]) and styrene (E_{T1} = 254 kJ mol^{-1} [55]) (Figure S22), or the triplet sensitizer benzophenone. The positions of the emission bands also remain independent of both the photocatalyst concentration and excitation wavelength. The emissive state of PCF is thus argued to be the first-excited singlet state ^{1}PCF*(S_1), in accordance with Kasha's rule. This assignment is supported by TEAS and TVAS measurements discussed below. The solvatochromism is consistent with a ^{1}PCF*(S_1) state of intramolecular CT character, whereas the solvent-independent emission behaviour of PCH points to an emissive state of LE character.[43] The TEAS measurements for PCH reported later show evidence of slow evolution of the S_1 to the T_1 state, which suggests contributions to emission from both ^{1}PCH*(S_1) and ^{3}PCH*(T_1), but prior reports indicate that this emission is not affected by the presence of oxygen.[56-57] Because our transient absorption

spectroscopy measurements establish the timescale for intersystem crossing, no further quenching studies of the PCH emission were carried out.

Locating reactive intermediates

The transient vibrational absorption (TVA) spectra presented in **Figure 1(a)**, and obtained over the 1530 – 1680 cm^{-1} region, highlight a band corresponding to a ring motion of $^{1}PCF^{*}(S_1)$ (1548 cm^{-1}) and a bleach from the photoinduced depletion of the ground state $^{1}PCF(S_0)$ (1600 cm^{-1}) (Figure S1). The absence of recovery of the bleach feature is ascribed to an overlapped transient absorption from a second ring breathing mode of $^{1}PCF^{*}(S_1)$. Combined TVAS and TEAS experiments (Figures S1 and S2) showed that the $^{1}PCF^{*}(S_1)$ state: (i) is fully populated within 2 ps *via* ultrafast internal conversion from the nascent excited state $^{1}PCF^{*}(S_4)$; (ii) has an estimated lifetime in DCM of $\tau[^{1}PCF^{*}(S_1)] = 3 \pm 1$ ns; and (iii) decays primarily *via* internal conversion or fluorescence to $^{1}PCF(S_0)$, with no discernible intersystem crossing into the triplet manifold. No transient absorptions from other species – namely $^{3}PCF^{*}(T_1)$ – were detected in any region. Upon the addition of methyl 2-bromopropionate (MBP), two new transient absorptions arise at 1553 cm^{-1} and 1660 cm^{-1}. These features are consistent with computed vibrational frequencies for the photocatalyst radical cation $^{2}PCF^{\cdot+}(D_1)$ (1551 cm^{-1}) and the debrominated radical fragment $^{2}MP\cdot(D_1)$ (1659 cm^{-1}). Any loss of the bleach at 1600 cm^{-1} expected for partial $^{1}PCF(S_0)$ recovery is again masked by overlapping gain features from $^{1}PCF^{*}(S_1)$. Assignment of the $^{2}PCF^{\cdot+}(D_1)$ feature was confirmed by steady-state FTIR characterization, with thermally mediated oxidation of PCF in the presence of $FeCl_3$ (Figure S5). None of the transient features were observed in control experiments performed on solutions of MBP without the photocatalyst.

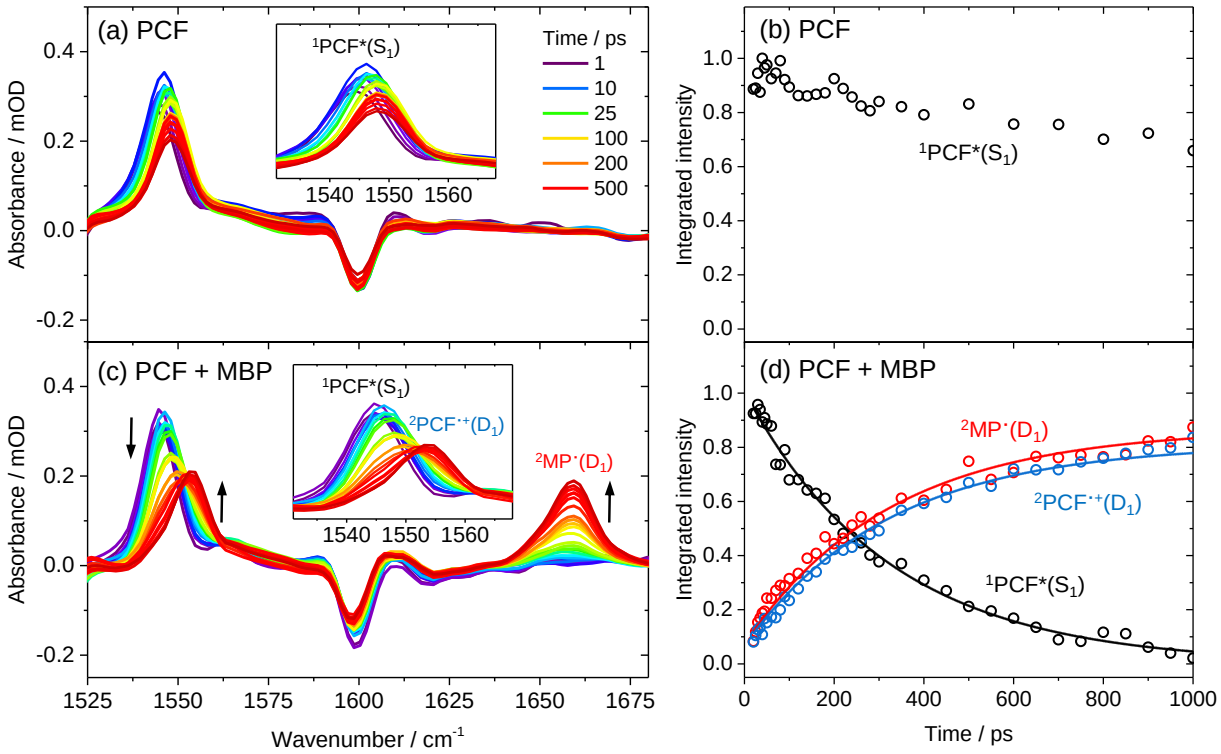

Figure 1: TVAS measurement of electron transfer rates for PCF, with TVA spectra obtained over the wavenumber range 1525 – 1680 cm^{-1} following pulsed photoexcitation at 370 nm. (a) TVA spectra for PCF (2.1 mmol dm^{-3}) in DCM; (b) the corresponding kinetic trace for $^{1}PCF^{*}(S_1)$ in the absence of MBP (○), obtained from integration of a Gaussian function fitted to the $^{1}PCF^{*}(S_1)$ absorption band (with floating center) at each time delay. (c) TVA spectra for PCF (2.1 mmol dm^{-3}) and MBP (0.9 mol dm^{-3}) in DCM; and (d) the corresponding time-dependent band intensities for $^{1}PCF^{*}(S_1)$ (○), $^{2}PCF^{\cdot+}(D_1)$ (○) and $^{2}MP^{\cdot}(D_1)$ (○), obtained from decomposition of the spectra in (c). Solid lines are fits to a concerted kinetic model for PET discussed in the main text. The absence of bleach recovery in (a) is attributed to the presence of an overlapped transient absorption by $^{1}PCF^{*}(S_1)$

Global fitting of all three integrated band intensity traces in **Figure 1(d)** to a single time constant is satisfactory (e.g. 324 ± 10 ps, [MBP] = 0.9 mol dm^{-3}), showing that: (i) $^{1}PCF^{*}(S_1)$, rather than $^{3}PCF^{*}(T_1)$, is indeed responsible for electron donation, because there is no kinetic evidence for an $S_1 \rightarrow T_1$ step; (ii) the electron transfer out-competes concomitant photophysical relaxation to $^{1}PCF(S_0)$; (iii) dissociation of bromide is sufficiently rapid that it cannot be experimentally distinguished from the electron transfer with our methods; and (iv) there is no significant thermal back-electron transfer from $^{2}MP^{\cdot}$ or Br^{-} to $^{2}PCF^{\cdot+}$ on the timescale of our measurements (a deduction confirmed by the persistance of $^{1}PCF(S_0)$ bleach features in the TVA spectra). The third

point is consistent with prior demonstration of concerted carbon-halogen bond dissociation by electron attachment,[58] and is further supported by the absence of an absorption signature for the geminate radical anion ^{2}MBP$^{\cdot-}$(D_1). It seems likely such a species would have a vibrational signature distinct from ^{2}MP$^{\cdot}$(D_1), especially in the carbonyl stretching mode, given the fundamental differences in the charges of the species and the hybridization of the α-carbon. We therefore represent the electron transfer process kinetically by a single step:

$$^1\text{PCF}^*(S_1) + \text{MBP} \rightarrow {}^2\text{PCF}^{\cdot+}(D_1) + \text{Br}^- + {}^2\text{MP}^{\cdot}(D_1) \qquad (1)$$

Tracking the PET: PCH *vs* PCF

Having located a spectroscopic signature of the ^{2}MP$^{\cdot}$(D_1) radical, its formation was tracked for a series of solutions with different concentrations of MBP (**Figure 2**) and the kinetics fitted to a dissociative PET model with a pseudo first-order rate coefficient $k'_{PET} = k_{PET}[MBP]$. No decay pathways for ^{2}MP$^{\cdot}$(D_1) were included in our kinetic model because the radical is not consumed on our timescale. The resulting pseudo first-order kinetic plot (**Figure 2a** inset) is linear, and affords a bimolecular rate coefficient of k_{PET}(PCF) = $(3.9 \pm 0.2) \times 10^9$ dm^3 mol^{-1} s^{-1}. Although fast, the PET appears to remain under activation control. This result was re-examined with TEAS by plotting the pseudo first-order rate coefficient for ^{1}PCF*(S_1) decay as a function of [MBP] (Figure S19); in agreement with the TVAS measurements, a bimolecular rate coefficient of k_{PET}(PCF) = $(4.4 \pm 0.3) \times 10^9$ dm^3 mol^{-1} s^{-1} was obtained. A more sophisticated kinetic model, accounting for static quenching at early times, is considered below. The linearity of the inset plots in Figure 2 (and Figure S19 of SI) indicates that the electronic-spin character of the electron-donating excited state of PCF* is not affected by intermolecular spin-orbit interactions with the Br atom in MBP.

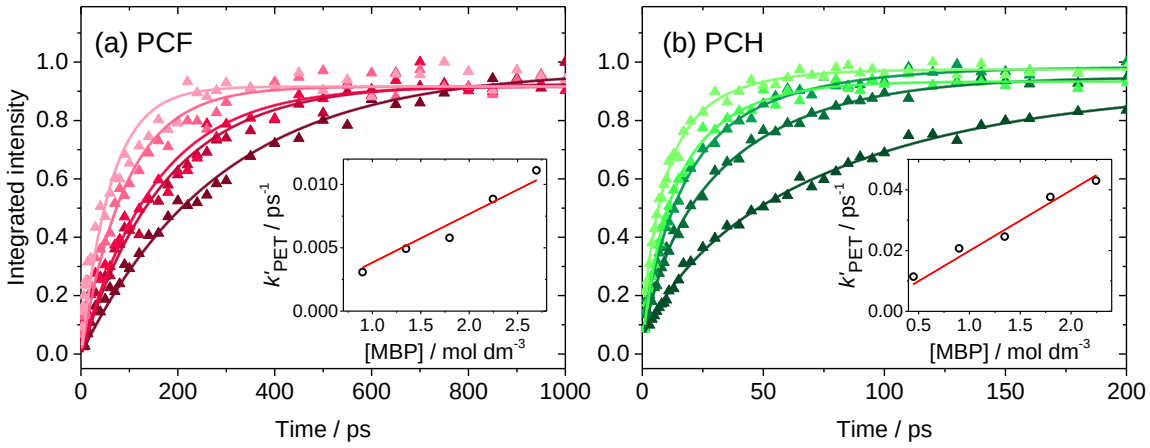

Figure 2: Rates of production of ^{2}MP·(D$_1$) radicals by electron transfer from the photocatalyst. TVAS concentration dependence study for: (a) PCF (2.1 mmol dm^{-3}) and MBP in DCM; and (b) PCH (2.1 mmol dm^{-3}) and MBP in DCM. Pseudo first-order kinetic plots are inset. The solid lines represent single exponential fits for PCF and biexponential fits for PCH (see main text for details).

Miyake and co-workers argued that PET from a photocatalyst such as PCF with excited state CT character should be faster than from structural analogues with an excited state of LE character, with consequent greater control over polymerization.[40-41] To test this suggestion, we also examined the photochemical dynamics of PCH and MBP in DCM. In the absence of MBP, the lifetime of the ^{1}PCH*(S$_1$) state in DCM is of the order of a few nanoseconds, and appears similar to ^{1}PCF*(S$_1$) (Figure S20). However, there is one notable difference: whereas the ^{1}PCF*(S$_1$) state decays to the ground-state without perceptible intersystem crossing into the triplet manifold, the decay of the ^{1}PCH*(S$_1$) state coincides with the concomitant growth of a new transient absorption centered on 450 nm (Figure S20). The position of this feature is inconsistent with the absorption signature of the radical cation ^{2}PCH·$^{+}$(D$_1$), indicating that there is no PET from photoexcited PCH to DCM, and we instead assign the new feature to a triplet state ^{3}PCH*(T$_1$). The quantum yield for PCH ISC was previously measured to be 0.26 in 3-methylpentane solution at 77 K, supporting our assignment.[59] In the presence of MBP a clear transient absorption from ^{2}MP·(D$_1$) was again observed (Figure S18) on timescales faster than T$_1$ growth, with a concentration dependence study affording an estimated bimolecular rate coefficient of k_{PET}(PCH) = (3.6 ± 0.2) × 10^{10} dm^{3} mol^{-1} s^{-1}. As with PCF, electron transfer appears to occur from the first excited singlet state, ^{1}PCH*(S$_1$) under our experimental conditions.

At the relatively high initiator concentrations (0.4 – 2.2 mol dm^{-3}) considered herein, our assumption of pseudo first-order kinetics is an approximation. The rate coefficient for the PET will in truth be time-dependent, because of a contribution from static quenching at early times.[24] The kinetics in the case of PCF are well fitted by mono-exponential functions, indicating that a simple pseudo first-order approach is appropriate. In the case of PCH, however, curvature in semi-logarithmic plots (Figure S16) suggests that time-dependent kinetics ought to be considered. Vauthey and co-workers used a formal diffusion model to deduce intrinsic rate coefficients for bimolecular electron transfers with both static and diffusive quenching contributions,[51] but here we adopt a simpler procedure governed by the available data, in which the kinetics are fitted with bi-exponential functions. The larger rate coefficients k'_{PET}(Stat) are ascribed to the static PET (7 – 17 ps), which might include ET within weakly associated PC-MBP complexes, whereas the smaller rate coefficients k'_{PET}(Dif) describe the diffusive PET. The bimolecular rate coefficient k_{PET} may then be obtained by plotting k'_{PET}(Dif) as a function of [MBP]; using this method, a marginally lower rate coefficient of k_{PET}(PCH) = $(2.0 \pm 0.2) \times 10^{10}$ dm^3 mol^{-1} s^{-1} was obtained. By focusing hereafter on the concentration-dependent, diffusional component of the bimolecular reaction kinetics, our discussion excludes possible contributions from association complexes of the photocatalyst and MBP.

Irrespective of the model invoked to analyse the kinetics, the primary conclusion remains unchanged: the rate of PET is 5 – 10 times greater for PCH than PCF, indicating that the ^{1}PCF*(S_1) state, of CT character, undergoes *slower* PET. Electron transfer from ^{1}PCH*(S_1) appears to be limited by the diffusion-controlled rate coefficient, estimated to be ~ 1.6×10^{10} dm^3 mol^{-1} s^{-1} in DCM.[54]

Marcus-Savéant theory states that the free energy barrier for a concerted dissociative electron transfer reaction $\Delta_{PET}G^{\ddagger}$ is related to the free energy change for the transfer $\Delta_{PET}G$, the bond dissociation energy E_{BD} and the solvent reorganization energy λ_0 according to:[60]

$$\Delta_{PET}G^{\ddagger} = \frac{\lambda_0+E_{BD}}{4}\left(1+\frac{\Delta_{PET}G}{\lambda_0+E_{BD}}\right)^2 \approx \frac{E_{BD}}{4}\left(1+\frac{\Delta_{PET}G}{E_{BD}}\right)^2 \quad (2)$$

To a good approximation the bond dissociation energy dominates the reorganization energy, leading to a simpler expression that depends exclusively upon E_{BD} and $\Delta_{PET}G$. The steady-state emission spectra of the two photocatalysts in DCM show that the ^{1}PCF*(S_1) state [λ_e^{max} (DCM) =

562 nm, 213 kJ mol^{-1}] is lower in energy than ^{1}PCH*(S_1) [λ_e^{max} (DCM) = 480 nm, 249 kJ mol^{-1}], relative to the respective ground-state photocatalysts, and KS-DFT calculations show that the ^{2}PCF$^{\cdot+}$(D_1) radical cation (436 kJ mol^{-1}) is higher in free energy than ^{2}PCH$^{\cdot+}$(D_1) (421 kJ mol^{-1}). That is to say, PCF has a more stable excited donor state and less stable radical cation compared to PCH, leading to an estimated difference in the PET driving force for the two photocatalysts of $\Delta\Delta_{PET}G = \Delta_{PET}G(PCF) - \Delta_{PET}G(PCH)$ = 51 kJ mol^{-1}. The Coulombic correction term present in the Weller equation, used to compute $\Delta_{PET}G$, is unlikely to differ to such a significant degree for the same solvent and electron acceptor, particularly given the structural similarity of the two photocatalysts.[61] Thus, the faster PET of PCH is consistent with Marcus-Savéant theory outside the inversion region, with approximate computations (outlined in the SI) affording k_{PET}(PCH) = 1.3 × 10^{11} dm^3 mol^{-1} s^{-1} and k_{PET}(PCF) = 1.6 × 10^9 dm^3 mol^{-1} s^{-1}. These values are in good agreement with the observed diffusion-control in PCH and activation-controlled rate in PCF, but may be underestimates if the MP· radical and Br$^-$ products form association complexes in solution.[62]

To assess the role of solvent and consider catalytically relevant conditions, the photophysical relaxation pathways of PCF and PCH were also investigated in DMF, which represents a typical solvent for O-ATRP.[40] In the case of PCF in DMF, in the absence of the initiator, both TEAS and TVAS show quenching of ^{1}PCF*(S_1), and in particular, TVAS indicates ^{1}PCF(S_0) ground-state recovery with a time constant of 677 $\pm$ 35 ps (**Figure 3**). No electronic or vibrational absorption signature of the radical cation ^{2}PCF$^{\cdot+}$(D_1) was observed, confirming no electron transfer to DMF, nor was there any evident branching into the triplet manifold. We estimate a T_1 quantum yield of less than 10% from analysis of the decays in Fig. 3(b). Accordingly, we assign this substantially reduced lifetime of ^{1}PCF*(S_1) in DMF to a rapid internal conversion to ^{1}PCF(S_0) ground-state; comparable examples are known for quenching of an excited state with intramolecular CT character in polar solvents.[63] Even with added benzophenone (1.0 M) as a triplet sensitizer, TEA spectra of solutions of PCF in DMF showed no evidence for formation of ^{3}PCF*(T_1) (see Figures S23 and S24). In contrast, the ^{1}PCH*(S_1) state has a lifetime in DMF that is beyond the range of our experimental setup, and the growth of a new transient absorption on the nanosecond timescale suggests competitive intersystem crossing to ^{3}PCH*(T_1), as in DCM (Figure S20).

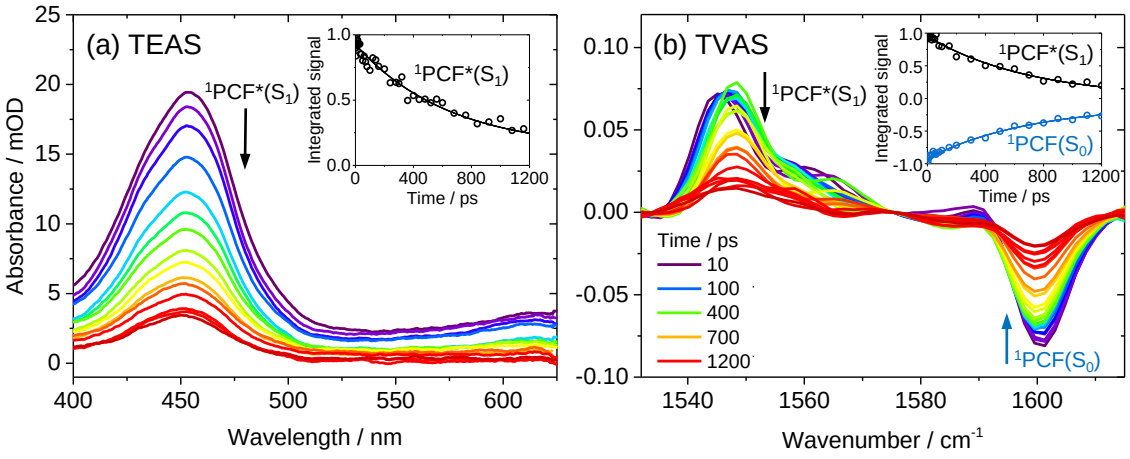

Figure 3: Photochemical dynamics of PCF in DMF. Transient electronic (a) and vibrational (b) absorption spectra of PCF (2.1 mmol dm^{-3}) in DMF following pulsed photoexcitation at 370 nm are shown, alongside the corresponding kinetic traces of ^{1}PCF*(S$_1$) and the ground state ^{1}PCF(S$_0$), obtained from integrating the fitted band intensities at each time. Global fitting affords a single time constant for ^{1}PCF*(S$_1$) → ^{1}PCF(S$_0$). The decay of ^{1}PCF*(S$_1$) is considerably faster than in DCM, indicating more efficient singlet quenching by DMF.

PCF is reported to be superior to PCH as a photocatalyst for controlling polymer molecular weight and dispersity in O-ATRP.[40-41] A robust mechanistic understanding of this selective control of O-ATRP must consider both the dissociative PET step which is the focus of this study, and the loss of radicals by the TET process illustrated in **Scheme 1**, because a combination of the two ET steps controls the radical concentration and hence the degree of polymer dispersity. Under otherwise identical conditions, the combination of slower PET from ^{1}PC*(S$_1$), and more energetically favourable TET (see **Scheme 1**) recovering ^{1}PC(S$_0$) from ^{2}PC$^{\cdot+}$ for PCF than for PCH,[40] will result in lower ^{2}PC$^{\cdot+}$ and organic radical concentrations when PCF is the chosen photocatalyst. The concentration of photoactive PC molecules is expected to decrease during polymerization because of the formation of ionic complexes (^{2}PC$^{\cdot+}$Br$^-$), with further consequences for the steady state radical concentration. The equilibrium constant for the formation of these complexes will depend on the solvent and PC used.[43, 45] Nevertheless, our comparison of the photochemical dynamics of PCH and PCF in DCM and DMF, and the known performances of the two PCs in O-ATRP,[40] lead us to suggest that the superior polymer dispersity control resulting from PCF use is a consequence of lower steady-state radical concentrations. We hypothesize that *short-lived* ^{1}PC*(S$_1$) states, *low* ISC quantum yields and *slower* PETs can be desirable properties for photoredox organocatalysts

in O-ATRP if low polymer dispersity is desired. In the case of PCF, these three photochemical characteristics work in concert to supress the production of the reactive dehalogenated radical under constant irradiation conditions, and low radical concentration is critical to controlled polymerization, as discussed by Matyjaszewski and coworkers.[48]

The proposed desirability of low ISC yields rests on the assumption that any populated $^3PC^*(T_1)$ state will be considerably longer-lived than $^1PC^*(S_1)$, and of sufficiently high energy that electron transfer out-competes further ISC or phosphorescence back to the $^1PC(S_0)$ ground-state. Efficient, high quantum-yield ISC to a long-lived $^3PC^*(T_1)$ will favor radical production at lower initiator concentrations, leading to poorer control during polymerization. In accordance with Marcus-Savéant theory, the PET rate can be moderated by seeking catalysts with comparatively stable excited donor states and unstable radical cations. Moreover, if the excited state of a given photocatalyst has CT character, the rate of PET can be slowed by employing solvents that preferentially stabilise the excited emissive state.

Our analysis of PC properties applies specifically to O-ATRP PC design, and is based solely on evidence from study of the electron transfer rates for two of the N,N-diaryl-5,10-dihydrophenazine PCs employed by Miyake and co-workers. Quantitative understanding of the optimum conditions for use of these and other PCs in O-ATRP requires knowledge of the rate coefficients for the numerous competing pathways and sequential steps in the polymerization process. Empirical investigations are currently more tractable; for example, Ryan *et al*. recently examined the optimization of irradiation intensity.[44] For ATRP using the metal complex photocatalyst *fac*-[$Ir(ppy)_3$], which is known to have an ISC quantum yield close to unity, Fors and Hawker found that decreasing the PC load from 0.2 mol% to 0.005 mol% significantly reduced the product polymer dispersity.[64] The low PC loads in this study, compared to the 0.5 mol% values for organic PCs typical in the O-ATRP system investigated by Miyake and co-workers, can be qualitatively explained by the different ET and ISC efficiencies of the two PCs: the high yield of long-lived T_1 states of *fac*-[$Ir(ppy)_3$] maintains radical concentrations appropriate for ATRP with low polymer dispersity at much lower PC concentrations than the organic PCs which have smaller ISC quantum yields, and therefore favor ET from shorter lived S_1 states. This interpretation is supported by the reported ISC quantum yield of only 2% for N,N-5,10-di(2-naphthalene)-5,10-dihydrophenazine,[65] as well as the ultrafast transient absorption spectroscopy measurements we report here.

PET and Solvent Effects

To further test the conclusions from our study, the effect of solvent on the rate of PET from the PCF and PCH photocatalysts was investigated with transient electronic absorption spectroscopy. The TEA spectra in **Figure 4** were obtained for PCH and PCF solutions of [MBP] = 1.8 mol dm^{-3} in DCM, toluene and DMF. There is no evidence from these spectra that addition of the bromine-containing MBP promotes ISC from the $^1PC(S_1)$ to the $^3PC(T_1)$ state. The time constants τ'_{PET} reported in the figure correspond to the pseudo first-order time constants for electron transfer, obtained using mono-exponential fits for PCF and bi-exponential fits for PCH, as discussed earlier. In each case, the initial spectrum at 2 ps is assigned to the $^1PC^*(S_1)$ state, whereas the 1200-ps final spectrum corresponds to the absorption signature of the radical cation $^2PC^{\cdot+}(D_1)$, as confirmed by steady-state UV-Vis characterization following thermally mediated oxidation of PCF by $FeCl_3$ (Figure S5 and S6)**.**

The absorption signatures of the $^1PC^*(S_1)$ states for the two photocatalysts are strikingly different, with the broad absorption extending beyond 625 nm in the case of PCH tentatively assigned as an excitation from $^1PCH^*(S_1)$ to the CT A_u state ($^1PCH^*(S_3)$ in the Franck-Condon region). For such a concentration of MBP, τ'_{PET} is well-approximated by the observed time constant for the decay of the $^1PC^*(S_1)$ state, τ_{obs}, with the exception of PCF in DMF. In this case, the decay of the $^1PCF^*(S_1)$ state in the absence of MBP – quantified by the time constant τ_1 = 677 ps (**Figure 3**) – is competitive with the PET, such that:

$$\tau'_{PET} = \frac{\tau_{obs}}{1-\frac{\tau_{obs}}{\tau_1}} \qquad (3)$$

For PCH, τ'_{PET} is essentially invariant over the three solvents, which is consistent with electron transfer being diffusion-limited. Subtle variations are likely to be a consequence of small modulations in the ground-state redox potentials. In the case of PCF, τ'_{PET} is inversely correlated with the energy of the $^1PCF^*(S_1)$ state [λ_{max}(Emission) = 585 nm (DMF), 562 nm (DCM), 508 nm (toluene)]. The reduction potentials of $^2PCF^{\cdot+}(D_1)$ and MBP will also depend upon the polarity of the solvent, but it is noteworthy that the observed trend in the PET rate is consistent with the trend in the $^1PCF^*(S_1)$ energy. Although solvent effects modulate the rate of PET in the case of PCF, as

is expected for an excited donor state of CT character, it is apparent that substituent effects (-H *vs* -CF_3) dominate the photochemical dynamics.

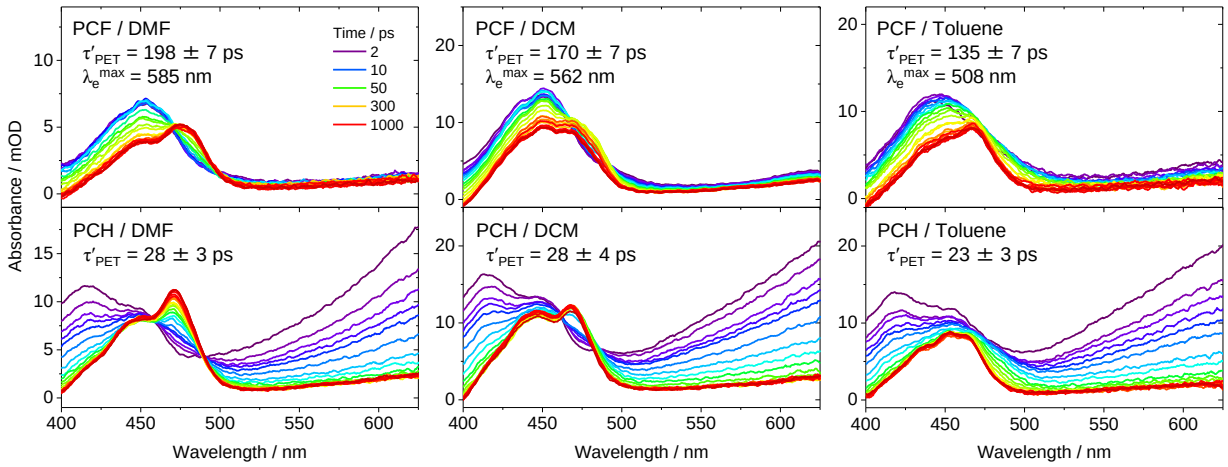

Figure 4: Solvent effects on the photochemical dynamics of PCF (top) and PCH (bottom) in the presence of MBP initiator after pulsed photoexcitation at 370 nm. DMF (left), DCM (middle) and toluene (right) solutions were examined, with PCF or PCH (2.1 mmol dm^{-3}) and MBP (1.8 mol dm^{-3}). The wavelength of maximum emission for PCH λ^{e}_{max} = 480 nm remains largely independent of solvent, due to the LE character of the ^{1}PCH*(S_1) state, whereas λ^{e}_{max} in the case of PCF is sensitive to solvent polarity due to the CT character of ^{1}PCF*(S_1). The time constants shown for PCH correspond to the slower k'_{PET}(Dif) components obtained by biexponential fits, as discussed in the main text.

Conclusions

The photochemical dynamics of initiation in O-ATRP have been probed with transient electronic and vibrational absorption spectroscopy, using two complementary N,N-diaryl-5,10-dihydrophenazine photoredox organocatalysts (PCF, PCH) and methyl 2-bromopropionate (MBP) as a representative radical initiator. For PCF, we report direct spectroscopic observation of a bimolecular dissociative photoinduced electron transfer from ^{1}PCF*(S_1) to MBP in DCM, with ^{1}PCF(S_0), ^{1}PCF*(S_1), ^{2}PCF$^{\cdot+}$(D_1) and ^{2}MP$^{\cdot}$(D_1) tracked simultaneously in real-time from the temporal evolution of their absorption signatures. Global fitting of the kinetics, and the absence of a distinct transient absorption for the geminate radical anion ^{2}MBP$^{\cdot-}$(D_1), indicate that electron transfer and bromide dissociation steps cannot be distinguished on our timescale. Studies of MBP concentration dependence with TVAS and TEAS in DCM afford a mean bimolecular rate

coefficient of k_{PET}(PCF) = (4.2 ± 0.4) × 10^9 dm^3 mol^{-1} s^{-1}. No spectroscopic trace of ^{3}PCF*(T_1) was detected within the temporal range of the experiment (1.3 ns) in either DCM or DMF; in the absence of MBP, the recovery of ^{1}PCF(S_0) accounts completely for the decay of ^{1}PCF*(S_1). The lifetime of the ^{1}PCF*(S_1) state is particularly short in DMF (677 ± 35 ps), which is significant as this represents a typical solvent for O-ATRP. In accordance with Marcus-Savéant theory, the rate of PET to MBP is activation-controlled and varies with the energy of the ^{1}PCF*(S_1) state, which is sensitive to solvent polarity on account of its intramolecular CT character.

Under the same conditions, a bimolecular rate coefficient of k_{PET}(PCH) = (2.0 ± 0.2) × 10^{10} dm^3 mol^{-1} s^{-1} was determined for PET from the ^{1}PCH*(S_1) state to MBP. This is ~5 times faster than the PCF and comparable to the diffusion-limited rate coefficient in DCM under ambient conditions. Contrary to the postulate of Miyake and co-workers, we thus find that PCH undergoes *faster* PET than PCF, despite the local excitation character of the ^{1}PCH*(S_1) state. The disparity in the rates of PET is more reliably explained with Marcus-Savéant theory, given the substantial difference in the estimated PET driving force of $\Delta\Delta_{PET}G = \Delta_{PET}G(PCF) - \Delta_{PET}G(PCH) \approx 51$ kJ mol^{-1}. In PCH, ISC to the first excited triplet state ^{3}PCH*(T_1) is competitive with fluorescence in both DCM and DMF; at the lower concentrations of MBP employed under synthetic conditions (0.05 – 0.10 mol dm^{-3}), therefore, it seems probable that electron transfer from ^{3}PCH*(T_1) is significant. Unlike PCF, the rate of PET remains independent of the solvent polarity, consistent with a diffusion-limited PET from an excited state of PCH of local excitation character.

Comparison of the photochemical dynamics of PCF and PCH suggests that a combination of *shorter* ^{1}PC*(S_1) lifetimes, *low* ISC quantum yields and *slower* PETs favors control of polymer molecular weight and dispersity in O-ATRP using these N,N-diaryl-5,10-dihydrophenazines as photocatalysts, by supressing the steady-state concentration of the dehalogenated radical. With this in mind, it would be prudent for synthetic chemists to consider the design of organocatalysts for O-ATRP that are characterized by short fluorescence lifetimes, low-lying excited donor states and high energy radical cations in a given solvent if control of polymer dispersity is a primary objective. Our results further suggest PET rates for *different* photocatalysts are better interpreted in terms of the free energies of excited states than their CT/LE electronic characters.

Acknowledgements

Financial support for this research from ERC Advanced Grant CAPRI 290966 is gratefully acknowledged. We thank Philip Coulter (University of Bristol) for help with the acquisition of some of the transient spectroscopy data.

Associated Content

Additional analysis, steady-state absorption and emission spectra, computational methodology, photocatalyst syntheses and TEAS/TVAS spectra and kinetics and are located in the Electronic Supporting Information.

Experimental Data

All experimental data are archived in the University of Bristol's Research Data Storage Facility (DOI 10.5523/bris.1wp4y75121tre2728hptf1hk55).

References

1. Nicewicz, D. A.; MacMillan, D. W. C., *Science* **2008,** *322*, 77-80.
2. Ischay, M. A.; Anzovino, M. E.; Du, J.; Yoon, T. P., *J. Am. Chem. Soc.* **2008,** *130*, 12886.
3. Narayanam, J. M. R.; Tucker, J. W.; Stephenson, C. R. J., *J. Am. Chem. Soc.* **2009,** *131*, 8756.
4. Prier, C. K.; Rankic, D. A.; MacMillan, D. W. C., *Chem. Rev.* **2013,** *113*, 5322-5363.
5. Shaw, M. H.; Twilton, J.; MacMillan, D. W. C., *J. Org. Chem.* **2016,** *81*, 6898-6926.
6. Karkas, M. D.; Porco, J. A.; Stephenson, C. R. J., *Chem. Rev.* **2016,** *116*, 9683-9747.
7. Nicholls, T. P.; Leonori, D.; Bissember, A. C., *Nat. Prod. Rep.* **2016,** *33*, 1248-1254.
8. Staveness, D.; Bosque, I.; Stephenson, C. R. J., *Acc. Chem. Res.* **2016,** *49*, 2295-2306.
9. Chen, J. R.; Hu, X. Q.; Lu, L. Q.; Xiao, W. J., *Acc. Chem. Res.* **2016,** *49*, 1911-1923.
10. Yoon, T. P., *Acc. Chem. Res.* **2016,** *49*, 2307-2315.
11. Ghosh, I.; Marzo, L.; Das, A.; Shaikh, R.; Konig, B., *Acc. Chem. Res.* **2016,** *49*, 1566-1577.
12. Goddard, J. P.; Ollivier, C.; Fensterbank, L., *Acc. Chem. Res.* **2016,** *49*, 1924-1936.
13. Ravelli, D.; Protti, S.; Fagnoni, M., *Chem. Rev.* **2016,** *116*, 9850-9913.
14. Takeda, H.; Ishitani, O., *Coord. Chem. Rev.* **2010,** *254*, 346-354.
15. Lang, X. J.; Zhao, J. C.; Chen, X. D., *Chem Soc Rev* **2016,** *45*, 3026-3038.
16. Skubi, K. L.; Blum, T. R.; Yoon, T. P., *Chem. Rev.* **2016,** *116*, 10035-10074.
17. Hopkinson, M. N.; Sahoo, B.; Li, J. L.; Glorius, F., *Chem. Eur. J.* **2014,** *20*, 3874-3886.
18. Hopkinson, M. N.; Tlahuext-Aca, A.; Glorius, F., *Acc. Chem. Res.* **2016,** *49*, 2261-2272.
19. Levin, M. D.; Kim, S.; Toste, F. D., *ACS Cent. Sci.* **2016,** *2*, 293-301.
20. Luo, J.; Zhang, J., *ACS Catal.* **2016,** *6*, 873-877.
21. Terrett, J. A.; Cuthbertson, J. D.; Shurtleff, V. W.; MacMillan, D. W. C., *Nature* **2015,** *524*, 330-334.
22. Zoller, J.; Fabry, D. C.; Ronge, M. A.; Rueping, M., *Angew. Chem. Int. Edit.* **2014,** *53*, 13264-13268.
23. Tsarevsky, N. V.; Matyjaszewski, K., *Chem. Rev.* **2007,** *107*, 2270-2299.
24. Arias-Rotondo, D. M.; McCusker, J. K., *Chem. Soc. Rev.* **2016,** *45*, 5803-5820.
25. Romero, N. A.; Nicewicz, D. A., *Chem. Rev.* **2016,** *116*, 10075-10166.
26. Margrey, K. A.; Nicewicz, D. A., *Acc. Chem. Res.* **2016,** *49* (9), 1997-2006.
27. Hari, D. P.; Konig, B., *Chem. Comm.* **2014,** *50*, 6688-6699.
28. Fukuzumi, S.; Ohkubo, K., *Chem. Sci.* **2013,** *4*, 561-574.
29. Ohkubo, K.; Fujimoto, A.; Fukuzumi, S., *J. Phys. Chem. A* **2013,** *117*, 10719-10725.
30. Ohkubo, K.; Mizushima, K.; Iwata, R.; Fukuzumi, S., *Chem. Sci.* **2011,** *2*, 715-722.
31. Romero, N. A.; Margrey, K. A.; Tay, N. E.; Nicewicz, D. A., *Science* **2015,** *349*, 1326-1330.
32. McManus, J. B.; Nicewicz, D. A., *J. Am. Chem. Soc.* **2017,** *139*, 2880-2883.
33. Romero, N. A.; Nicewicz, D. A., *J. Am. Chem. Soc.* **2014,** *136*, 17024-17035.
34. Pitre, S. P.; McTiernan, C. D.; Ismaili, H.; Scaiano, J. C., *ACS Catal.* **2014,** *4*, 2530-2535.
35. Pitre, S. P.; McTiernan, C. D.; Ismaili, H.; Scaiano, J. C., *J. Am. Chem. Soc.* **2013,** *135*, 13286-13289.
36. Ghosh, T.; Das, A.; Konig, B., *Org. Biomol. Chem.* **2017,** *15*, 2536-2540.
37. Meyer, A. U.; Wimmer, A.; Konig, B., *Angew. Chem. Int. Edit.* **2017,** *56*, 409-412.
38. Treat, N. J.; Sprafke, H.; Kramer, J. W.; Clark, P. G.; Barton, B. E.; de Alaniz, J. R.; Fors, B. P.; Hawker, C. J., *J. Am. Chem. Soc.* **2014,** *136*, 16096-16101.
39. Miyake, G. M.; Theriot, J. C., *Macromolecules* **2014,** *47*, 8255-8261.

40. Theriot, J. C.; Lim, C. H.; Yang, H.; Ryan, M. D.; Musgrave, C. B.; Miyake, G. M., *Science* **2016,** *352*, 1082-1086.
41. Pearson, R. M.; Lim, C. H.; McCarthy, B. G.; Musgrave, C. B.; Miyake, G. M., *J. Am. Chem. Soc.* **2016,** *138*, 11399-11407.
42. Wang, J. S.; Matyjaszewski, K., *J. Am. Chem. Soc.* **1995,** *117*, 5614-5615.
43. Lim, C. H.; Ryan, M. D.; McCarthy, B. G.; Theriot, J. C.; Sartor, S. M.; Damrauer, N. H.; Musgrave, C. B.; Miyake, G. M., *J. Am. Chem. Soc.* **2017,** *139*, 348-355.
44. Ryan, M. D.; Pearson, R. M.; French, T. A.; Miyake, G. M., *Macromolecules* **2017,** *50*, 4616-4622.
45. Ryan, M. D.; Theriot, J. C.; Lim, C. H.; Yang, H. S.; Lockwood, A. G.; Garrison, N. G.; Lincoln, S. R.; Musgrave, C. B.; Miyake, G. M., *J. Polym. Sci. Pol. Chem.* **2017,** *55*, 3017-3027.
46. Discekici, E. H.; Treat, N. J.; Poelma, S. O.; Mattson, K. M.; Hudson, Z. M.; Luo, Y. D.; Hawker, C. J.; de Alaniz, J. R., *Chem. Commun.* **2015,** *51*, 11705-11708.
47. Jockusch, S.; Yagci, Y., *Polym. Chem.* **2016,** *7*, 6039-6043.
48. Pan, X. C.; Fang, C.; Fantin, M.; Malhotra, N.; So, W. Y.; Peteanu, L. A.; Isse, A. A.; Gennaro, A.; Liu, P.; Matyjaszewskit, K., *J. Am. Chem. Soc.* **2016,** *138*, 2411-2425.
49. Kumpulainen, T.; Lang, B.; Rosspeintner, A.; Vauthey, E., *Chem. Rev.* **2017,** *117*, 10826-10939.
50. Dereka, B.; Koch, M.; Vauthey, E., *Acc. Chem. Res.* **2017,** *50*, 426-434.
51. Rosspeintner, A.; Angulo, G.; Vauthey, E., *J. Am. Chem. Soc.* **2014,** *136*, 2026-2032.
52. Sun, Q. C.; Dereka, B.; Vauthey, E.; Daku, L. M. L.; Hauser, A., *Chem. Sci.* **2017,** *8*, 223-230.
53. Kellogg, R. E.; Simpson, W. T., *J. Am. Chem. Soc.* **1965,** *87*, 4230-&.
54. Montali, M.; Credi, A.; Pradi, L.; Gandolfi, M. T., *Handbook of Photochemistry*. 3rd ed.; CRC Press: Boca Raton, 2006.
55. Gorman, A. A.; Gould, I. R.; Hamblett, I., *J. Am. Chem. Soc.* **1981,** *103*, 4553-4558.
56. Evans, D. F., *J. Chem. Soc.* **1957**, 1351-1357.
57. Ni, T.; Caldwell, R. A.; Melton, L. A., *J. Am. Chem. Soc.* **1989,** *111*, 457-464.
58. Isse, A. A.; Gennaro, A.; Lin, C. Y.; Hodgson, J. L.; Coote, M. L.; Guliashvili, T., *J. Am. Chem. Soc.* **2011,** *133*, 6254-6264.
59. Morris, J. V.; Bruhlman, U.; Serafimov, O.; Huber, J. R., *Ber Bunsen Phys Chem* **1974,** *78*, 1348-1353.
60. Saveant, J. M., *J. Am. Chem. Soc.* **1987,** *109*, 6788-6795.
61. Rehm, D.; Weller, A., *Berich. Bunsen. Gesell.* **1969,** *73*, 834.
62. Cardinale, A.; Isse, A. A.; Gennaro, A.; Robert, M.; Saveant, J. M., *J. Am. Chem. Soc.* **2002,** *124*, 13533-13539.
63. Dereka, B.; Rosspeintner, A.; Li, Z. Q.; Liska, R.; Vauthey, E., *J. Am. Chem. Soc.* **2016,** *138*, 4643-4649.
64. Fors, B. P.; Hawker, C. J., *Angew. Chem. Int. Edit.* **2012,** *51*, 8850-8853.
65. Du, Y.; Pearson, R. M.; Lim, C. H.; Sartor, S. M.; Ryan, M. D.; Yang, H. S.; Damrauer, N. H.; Miyake, G. M., *Chem. Eur. J.* **2017,** *23*, 10962-10968.

Table of Contents Graphic